INVESTIGATION OF TURBULENT OXY-FUEL JET FLAMES USING SIMULTANEOUS LINE IMAGING OF RAMAN/RAYLEIGH LASER DIAGNOSTICS

Alexis Sevault[*], Robert S. Barlow[**], Matthew Dunn[**] and Mario Ditaranto[***]
alexis.sevault@ntnu.no
[*]Energy and Process Engineering Department, Norwegian University of Science & Technology, 7491 Trondheim, Norway.
[**]Combustion Research Facility, Sandia National Laboratories, Livermore, CA 94551-0969, USA.
[***]Department of Energy Processes, SINTEF Energy Research, 7465 Trondheim, Norway.

Abstract
An experimental study on turbulent non-premixed jet flames is presented with focus on CO_2-diluted oxy-fuel combustion in a coflow burner. Measurements of local temperatures and concentrations of the main species CO_2, O_2, CO, N_2, CH_4, H_2O and H_2 were achieved using the simultaneous line-imaged Raman/Rayleigh laser diagnostics setup at Sandia National Laboratories. Two series of flames burning mixtures of methane and hydrogen were investigated: in the first series, the hydrogen volume fraction in the fuel was varied from 37 to 55%, whereas in the second series the jet Reynolds number Re_{Fuel} was varied from 12,000 to 18,000. Besides local temperatures and concentrations, the results revealed insights on the progression of localized extinction in the near-field**.** The degree of extinction decreased with the hydrogen volume fraction and increased with the jet Reynolds number. Based on the pdf's of the temperature, an index able to quantify the degree of extinction in the present flames was calculated as a fully burning probability. A comparison of measured conditional mean mass fractions and laminar flame calculations underlined the significant level of differential diffusion in the near-field that tended to decrease farther downstream. The results also showed high local CO levels induced by the high content of CO_2 in the oxidizer and flame products.

Introduction
Due to climate change and favourable policies aiming at reducing carbon dioxide emissions, many technologies have been investigated as a transition between the current combustion-oriented energy production, generating undesirable emissions, and the renewable energy production. Based on the great advance in oxygen separation technologies, which leads to reduced costs and the absence of post-combustion constraints, oxy-fuel combustion stands for a potentially serious and efficient solution within this range. Bolland et al. [1, 2] and Tan et al. [3] studied the design of oxy-fuel gas turbines fired with natural gas and concluded that efficiency is best with combined cycle operation, i.e. with recycled CO_2 as a diluting gas. Using O_2/CO_2 mixtures instead of air for fuel combustion results in exhaust gases composed of water, which can be easily separated by condensation, and relatively pure carbon dioxide that can be captured, stored, and directly used for recycling in the power cycle. An advantage of this technology is its potential to reduce NO_x emissions, as shown by Ditaranto et al. [4-6]. It was also observed that NO_x emissions are especially influenced by air leaks and residual N_2 present in either natural gas or oxygen stream. However, NO_x emissions are lower with oxy-fuel combustion if CO_2 dilution is considered [7]. Another advantage gained over air-fuel combustion is the elimination of the capital and maintenance costs of air preheater by using combine cycle operation, as suggested by Boushaki et al. [8].

The heat transfer properties of CO_2 are radically different from those of N_2. Consequently, as Ditaranto et al. [9] observed, CO_2 molecules radiate much more than N_2 molecules and

tend to locally quench the chemical reaction. It has been seen in different studies [9, 10] that the molar percentage of oxygen in the oxidant should be around 30% to reach stabilized regimes, depending on the mixing process. In the present study, the oxygen content is set to 32% in the oxidizer mixture. Indeed, it has been observed during the first tests that even at low Reynolds number, simple jet flames barely sustained with less than 30% oxygen. However, Kutne et al. [11] stabilized oxy-fuel flames with contents as low as 20% oxygen in the oxidizer by using swirl to optimize the mixing. The choice of using a coflow in the present study has been motivated by the interest in observing how the turbulent mixing is characterized in CO_2-diluted oxy-fuel flames.

Another phenomenon that may affect the flame structure is the differential diffusion, which is especially likely to happen with high H_2 content in the fuel. Barlow et al. [12] showed that its magnitude in jet flames progressively decreases as the Reynolds number increases. Computational codes do not necessary take differential diffusion into account since they are most likely industry-oriented, where Reynolds numbers are much higher than those achievable in laboratories. Since one purpose of the present experiments is to provide data for validation of computational codes, the Reynolds numbers have been set to the highest reachable values in the laboratory conditions to minimize the effect of this phenomenon.

Besides limiting the flames series to stabilized conditions, laser Raman/Rayleigh scattering technique restricted the study to non-sooting flames, at least over most of their length. Indeed, fluorescence from fuel-rich zones, where soot is likely to form locally, alters Raman signals and, in some cases, floods them. The local soot level is actually very sensitive to the oxygen content in the oxidizer. In fact, this topic is currently being studied at SINTEF Energy Research in Norway. In the present case, thanks to the high H_2 content in the fuel, the level of interferences coming from soot formation was at an acceptable level so that the Raman and Rayleigh signals could be confidently corrected through calibration.

Specific Objectives

Literature regarding CO_2-diluted oxy-fuel flame structure and composition is scarce. The objectives of this study were to investigate the detailed scalar structure of CO_2-diluted oxy-fuel jet flames, exhibiting strong effects of turbulence chemistry interaction, and thereby provide new insights and data that may be used for improvement or validation of computational combustion codes.

Table 1. Flames properties.

Name	%H_2 in fuel	Re_{Fuel}	Jet speed (m/s)	Coflow speed (m/s)
A-1	55	15,000	98.2	0.778
A-2	45	15,000	84.5	0.755
A-3	37	15,000	75.8	0.739
B-1	55	12,000	78.6	0.622
B-2	55	15,000	98.2	0.778
B-3	55	18,000	117.8	0.933

Five flames were measured in order to parametrically determine the effects of fuel composition (CH_4/H_2 volume fraction) and jet Reynolds number on the degree of localized extinction measured in the flame. Localized extinctions have been recently studied by Barlow et al. [13] in piloted jet flames of CH_4/H_2/air, in comparable conditions. Accurate prediction of localized extinction is recognized as an important test of turbulent combustion models [14].

Two series of three flames were investigated (one flame is common to both series). Both series had an overall equivalence ratio of 1.25 and a molar percentage of O_2 in the oxidizer of

32%, based on volumetric flow rates of fuel and the CO_2/O_2 coflow. In the A-series, the molar percentage of H_2 in the fuel is varied from 37% to 55% with a constant jet Reynolds number Re_{Fuel} = 15,000. In the B-series, Re_{Fuel} is varied from 12,000 to 18,000 with a molar content of 55% H_2 in the fuel. Details are shown in Table 1.

Experimental Setup

Measurements were performed using the simultaneous line imaging of Raman/Rayleigh scattering. Details of the hardware configuration can be found in [15]. The setup enabled measurements of single-shot profiles of temperature and the mass fractions of all major species (CO_2, O_2, CO, N_2, CH_4, H_2O and H_2). The spatial resolution was 0.104 mm along a ~6 mm section of the focused beam. Total energy in the test section for the Raman/Rayleigh measurements was 1 J/pulse at 532 nm with an overall pulse duration of ~400 ns from three frequency-doubled Nd:YAG. Due to the high level of radiation emitted by CO_2 within the flames, heat-sensitive devices close to the flame were protected by reflective aluminium foil. The large collection lens in front of the Raman/Rayleigh setup was shielded by a 150-mm square, 1-mm thick window of infrared absorbing filter glass (Schott KG2).

Note that CO Laser Induced Fluorescence (LIF) line measurements and OH planar-LIF measurements were performed at the same time, but results are still being processed and thus not presented in the present paper.

Thanks to the H_2 content in the fuel, the flame remained attached to the fuel nozzle. The fuel nozzle was 5-mm inside diameter with 0.5 mm wall thickness and squared-off end. This was surrounded by a laminar coflow of 96.5 mm inside diameter. The nozzle had its tip 40 mm above the coflow and was long enough so that when the fuel mixture reached the nozzle tip the flow was considered fully developed. The oxidizer mixture first flowed through a series of perforated plates and then through a honeycomb to allow a uniform flow distribution. The burner was mounted at the top of a 25 cm x 25 cm square-section wind tunnel from where fresh air was flowing at 0.5 m/s to accompany the flow of interest and prevent early mixing with ambient air. The setup allowed measurements from 1 to 20 diameters above the nozzle with no mixing with ambient air, and thus, no intrusion of nitrogen within the probe volume. Thus, no combustion chamber was required for measurements in the near-field, which was most important for the present investigation of localized extinction in these flames.

The jet flames were axisymmetric and thus radial profiles were measured from a location slightly back from the central axis to the pure oxidizer region, to ensure capturing the full reaction zone. To obtain the profiles, the 6-mm probe was translated by steps of 3 mm where a minimum of 500 shots were systematically acquired. When crossing the reaction zone, as much as 1500 shots were recorded to improve the quality of the data.

The calibration and data processing method used for laser Raman scattering was the recently developed hybrid method. Detailed description can be found in [16]. The method is based on the Ramses spectra simulation code [17], which generates Raman spectral libraries for the major species over temperatures ranging from 290 K to 2500 K, for optically well characterized detection setups. Coupled with a short series of calibration measurements (practically one per species), most of the calibration coefficients required to process the Raman data can be known by integrating the spectral libraries over regions corresponding to the on-chip binning. However, not everything was solved by the Ramses code. Since the code is based on quantum mechanical models, spectra simulations for methane, for instance, are not available over the temperature range of interest. Thus, a few calibration coefficients still had to be found through direct measurements over a large temperature range.

Signals were corrected for CCD background, flat field, total Nd:YAG laser energy, interferences from laser induced fluorescence in Raman signals, broadband flame luminosity,

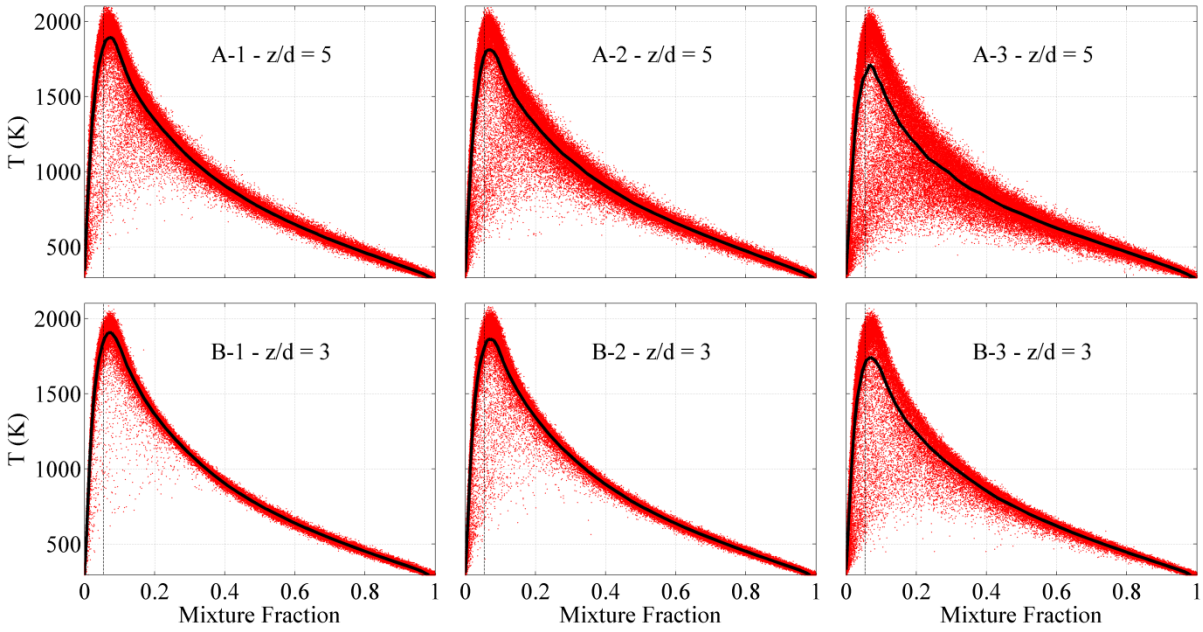

Figure 1. Scatter plots of Rayleigh temperature at z/d = 5 for A-series and at z/d = 3 for B-series. The conditional mean temperature is plotted with a solid line. The stoichiometric mixture fraction is marked by a vertical dashed line.

beam steering through flames, and bowing effect through Raman optics [16]. Data were filtered for sparks and dusts particles altering Rayleigh and Raman signals, although such events were rare since in-line particle filters had been installed along the critical gas lines.

As for performing laser diagnostics, CO_2-diluted oxy-fuel flames remained very challenging due to their high CO_2 content. For instance, compared to air, the molecule has a different refractive index, and this caused some steering of the laser beam when it passed through the unsteady interface between air and the CO_2/O_2 coflow. Another drawback is its radiative property that creates a significant thermal load in flame conditions. Those two examples had to be taken into account while performing the experiments. Beam steering was not severe using the 32% O_2 mixture, and the main effects of beam steering are accounted for automatically by the hybrid Raman/Rayleigh processing method [16].

Estimates of accuracy based on uncertainties in calibration flow conditions and repeatability of measurement are roughly equal to those shown in [15]. All flows were measured using mass flow controllers which were calibrated (within 1% of reading) against laminar flow elements. The mixture fraction was calculated from the measured mass fractions using the Bilger formulation [18].

Results and Discussion

Most of the following comments will deal with the progression of the flame structure in the A- and B-series of flames, and will rely on the analysis of Favre-average radial profiles of selected mass fractions, measured conditional scalar statistics in mixture fraction space, and results from laminar diffusion flame calculations. First, the focus will be set on the evolution of the localized extinction, followed by an investigation on the influence of differential diffusion. Then, the CO measurements and the measurement limits will be discussed.

Localized extinction

Localized extinction occurs when turbulent mixing rates between fuel and oxidizer become competitive with critical rates of chemical reactions. This leads to local temperatures drops due to increasing heat removal rates from convection and diffusion along with decreasing

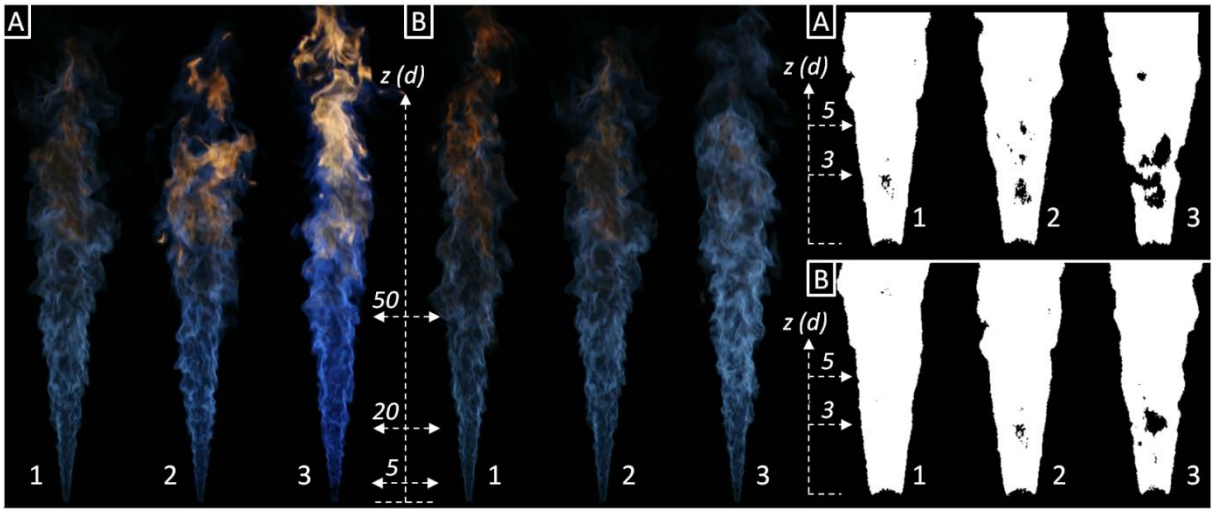

Figure 2. Pictures of A-series flames (left), B-series flames (centre) and close-ups from the region of localized extinction for A-series (top-right) and B-series (bottom-right). Close-ups were post-processed by applying a threshold to highlight the localized extinction. Exposure time: 1/2500 s, ISO: 1600.

chemical reaction rates.

Fig. 1 shows the scattered plots of Rayleigh temperature versus mixture fraction for both flame series. Dots scattered below the narrow, dense band of temperature indicate localized extinction. Barlow et al. [13] reported that extinction roughly took place around four diameters above the nozzle within the CH_4/H_2/air flames that were studied. Similarly, extinction tended to happen within this area in the present flame series. The probability of localized extinction gradually increased by lowering the H_2 content in fuel as seen with the A-series or by increasing Re_{Fuel} as seen with the B-series. Fig. 1 shows that the samples deviating from the narrow band of temperature were especially located between 600 and 1700 K and the evolution of probability of localized extinction did not significantly affect the behaviour of the narrow band of temperature, representing fully reacting states or flamelets. The conditional mean temperature, shown by red curves, decreases only moderately for the observed levels of localized extinction.

As shown in Fig. 2, Flames A-1 and B-1 visually appeared to be fully burning even though they displayed in Fig. 1 a non-negligible number of samples deviating from the narrow band of temperature. During the preliminary phase of defining the flame conditions, H_2 content of 60% in fuel was tested and displayed fewer samples out of the narrow band of temperature (not shown here).

The post-processing applied to the flame pictures allowed qualitative visualization of the localized extinction as areas of reduced luminosity (see Fig. 2, right). Its shape and exact location was constantly moving. The intense localized extinction from Flame A-3 could easily be seen as shown in Fig. 2 (top-right). As expected, by lowering the H_2 content in fuel below 37%, localized extinction systematically increased, leading to lift-off or flame blow-off. Similarly, increasing further Re_{Fuel} until levels around 20,000 also lead to lift-off and instabilities.

The conditional means of mass fraction for CO, H_2, O_2 and H_2O are plotted with the mixture fraction in Fig. 3 for both flame series, at three different axial positions intercepting the region of localized extinction. Similarly, the Favre-averaged mass fractions of CO, H_2, O_2 and H_2O are plotted with the radial position in Fig. 4. Note that, measurements performed at 1 diameter above the nozzle revealed mass fraction profiles very similar for each series and thus, are not shown here. By looking at O_2 mass fraction at 3 or 5 diameters above the fuel

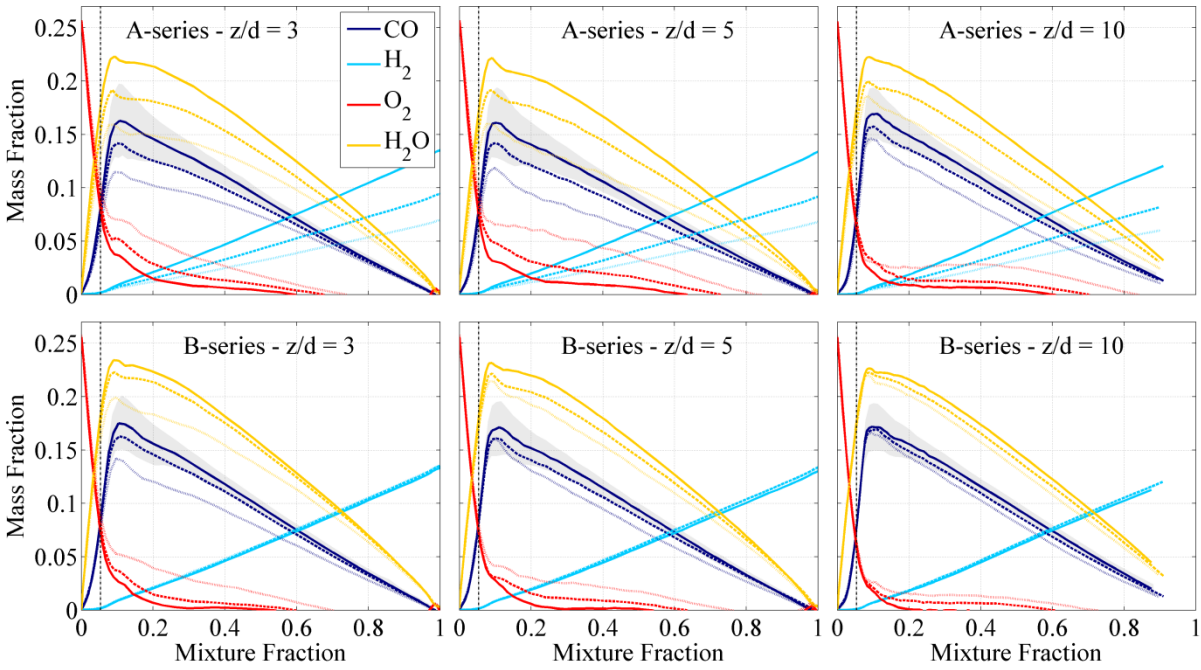

Figure 3. Conditional means for CO, H_2, O_2 and H_2O mass fractions for both A- and B-series at *z/d* = 3, 5 and 10. Flames A-1 and B-1 are shown with solid lines, A-2 and B-2 with dashed lines, and A-3 and B-3 with dotted lines. The stoichiometric mixture fraction is marked by a dashed line. The grey area represents the conditional rms fluctuations for CO mass fraction corresponding to the first flame of each series respectively.

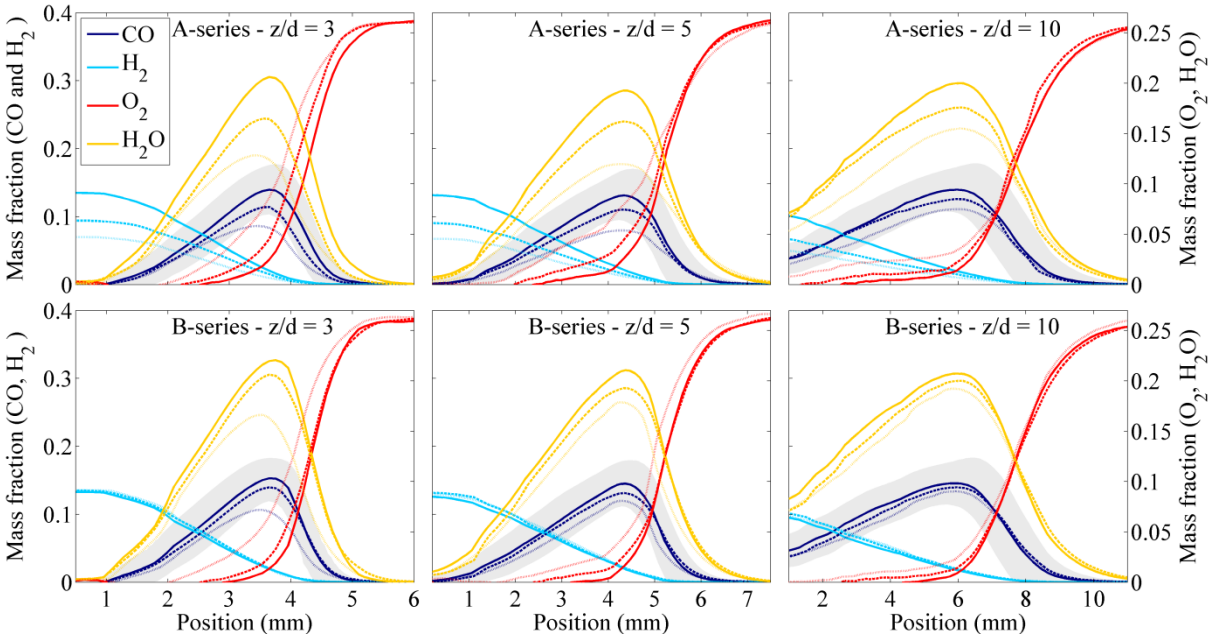

Figure 4. Favre-averaged radial profiles for CO, H_2, O_2 and H_2O mass fractions for both A- and B-series at *z/d* = 3, 5 and 10. Flames A-1 and B-1 are shown with solid lines, A-2 and B-2 with dashed lines, and A-3 and B-3 with dotted lines. The grey area represents the rms fluctuations (according to the Favre decomposition) for CO mass fraction corresponding to the first flame of each series respectively.

nozzle in Fig. 3 and 4, it can be seen on the fuel-rich side that unburnt oxidizer showed up into the jet with lower H_2 content in fuel or higher Re_{Fuel}. This was a direct consequence of localized extinction, which seemed to vanish out farther downstream. It also seemed that the

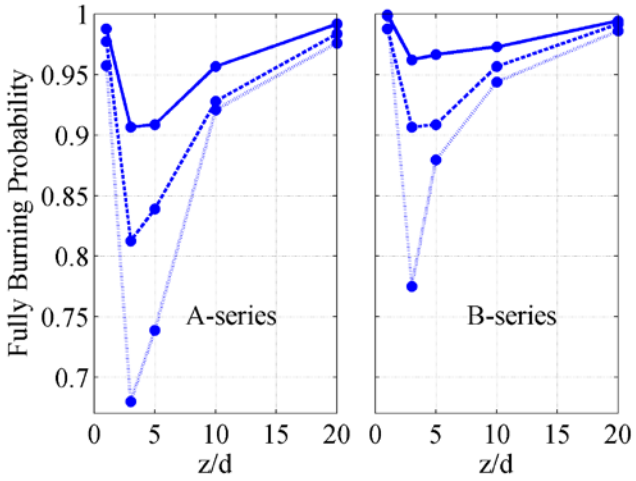

Figure 5. Fully burning probability plotted with axial location for both flame series, with T_{lim} = 1700 K and $\boldsymbol{\sigma}$ = 0.02. A-1 and B-1 are shown with solid lines, A-2 and B-2 with dashed lines, and A-3 and B-3 with dotted lines.

localized extinction was located slightly more upstream in the B-series when looking at the progression.

In Fig. 3 and 4, it appeared that levels of H_2O and CO gradually decreased around the localized extinction zone, respectively with decreasing the H_2 content in fuel in the A-series, and with increasing the jet Reynolds number in the B-series. This variation was mostly induced by the increase of O_2 mass fraction. However, this was slightly more intense in the A-series and could be explained by the variation of fuel composition, coupled with lower jet exit speeds. Farther downstream, far from the localized extinction, the decreased levels in H_2O and CO were still visible. A slight increase in CO_2 mass fraction was also found but is not shown here. As for the B-series, fuel and oxidizer compositions are the same for each flame. However the jet exit and coflow speeds were greatly varied, so that one can expect a decrease in the relative importance of molecular diffusion compared to turbulent transport. Barlow et al. [12] reported such a transition with piloted methane/air jet flames and showed that transitional effects of transport regimes especially appeared in the near-field and were vanished out further downstream, as it was also the case for the B-series. This topic is investigated in the following section.

One way to quantify the degree of extinction was to define a fully burning probability (FBP) (see Fig. 5). First, the probability-density function (pdf) of the temperature was calculated for each profile on a short bandwidth, 2σ, of mixture fraction centred on the locus of maximum temperature. Then, the pdf's corresponding to the temperatures above a reasonable arbitrary threshold temperature, T_{lim}, can be integrated and plotted with the measured axial locations. A flame showing an axial profile with a flat FBP equal to 1 would be considered as fully burning. T_{lim} = 1700 K seemed to be a reasonable temperature since it was well below the calculated adiabatic temperature (~2200 K for all the present flames) and still relatively high.

It can be seen in Fig. 5 that, according to the FPB criterion, none of the present flames was fully burning, though Flame B-1 was reasonably close. Fig. 5 also shows that localized extinction happened systematically between 1 and 5 diameters above the nozzle and its effect vanished out downstream since all profiles seemed to tend to FBP = 1. As expected, Flame A-3 appeared to have the most dramatic FBP of the two series, even though, only a few axial locations have been measured and a finer resolution would be required to draw concrete conclusions.

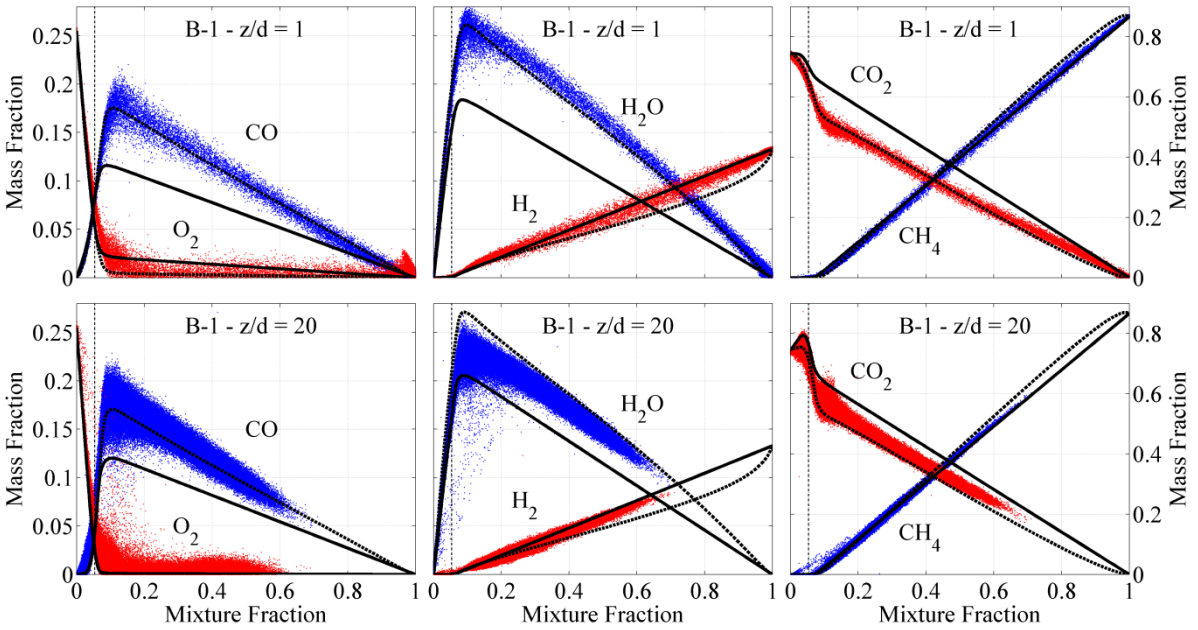

Figure 6. Scatter plots of mass fractions plotted versus the Bilger mixture fraction for Flame B-1 at z/d = 1 and 20. Corresponding results from laminar flame calculations for strain rates of 800 s^{-1} (top) and 15 s^{-1} (bottom) are plotted using the two different transport regimes: full multi-component transport (dash lines) and equal diffusivities (solid lines).

Influence of differential diffusion

To evaluate the influence of differential diffusion, laminar diffusion flame calculations were performed with CHEMKIN-PRO [19] using the opposed-jet reactor with the GRI 3.0 mechanisms [20]. Results were compared to the present flames using similar fuel and oxidizer compositions. In turbulent non-premixed jet flames, one could expect to match a location in the near-field with a relatively high strain rate whereas a location farther downstream would rather match with a lower strain rate [21]. Focusing especially on Flame B-1, supposed to be more relevant since closer to a fully burning state, and on CO mass fraction, a good match was found with a strain rate a = 800 s^{-1} at z/d = 1 and a = 15 s^{-1} at z/d = 20, as shown in Fig. 6, where results from the two different transport regimes were plotted: full multi-component transport and equal diffusivity. The full transport regime takes into account the effect of differential diffusion, whereas the equal diffusivity regime sets all species diffusivities equal to the thermal diffusivity (Lewis number equal to 1).

In turbulent non-premixed jet flames, the shear layer develops downstream by forming larger-scale turbulent structures until stirring the whole reaction zone so that those control the local mixing rates. Thus, the effects of differential diffusion are expected to be more significant closer to the nozzle, as reported from different flames burning hydrogen [22, 23]; whereas equal diffusivity would rather match far downstream zones where the upstream effects of differential diffusion have been washed out through a process of re-entrainment and turbulent mixing over the development length of the jet [21].

Fig. 6 shows the scatter plots of CO, O_2, H_2, H_2O, CO_2 and CH_4 mass fractions compared to the laminar flame calculations. At 1 diameter above the nozzle, most results agree well with the full transport regime, even though CH_4 and H_2 mass fractions seem to rather agree with the equal diffusivity regime. At 20 diameters above the nozzle, the results are settled between the two different regimes. However, the trend suggests that if measurements would have been performed even farther downstream, they might have best agreed with the equal diffusivity regime. Note that changing the strain rates would not alter these observations.

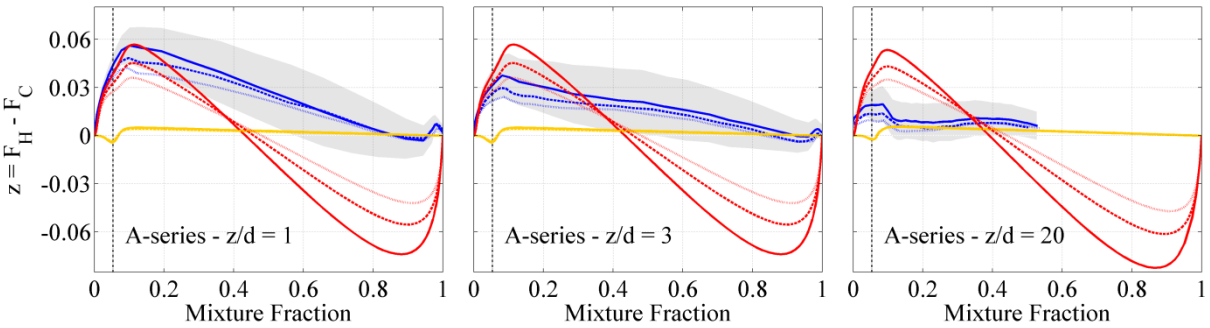

Figure 7. Differential diffusion parameter *z* plotted versus the Bilger mixture fraction for A-series flames at *z/d* = 1, 3 and 20. A-1 is shown with blue solid lines, A-2 with blue dashed lines, and A-3 with blue dotted lines. Corresponding results from laminar flame calculations using A-1 (solid lines), A-2 (dashed lines) and A-3 (dotted lines) fuel and oxidizer compositions with strain rates of 800 s^{-1} (left and centre) and 15 s^{-1} (right) are plotted using the two different transport regimes: full multi-component transport (red lines) and equal diffusivities (orange lines). The grey area represents the conditional rms fluctuations for *z* corresponding to Flame A-1.

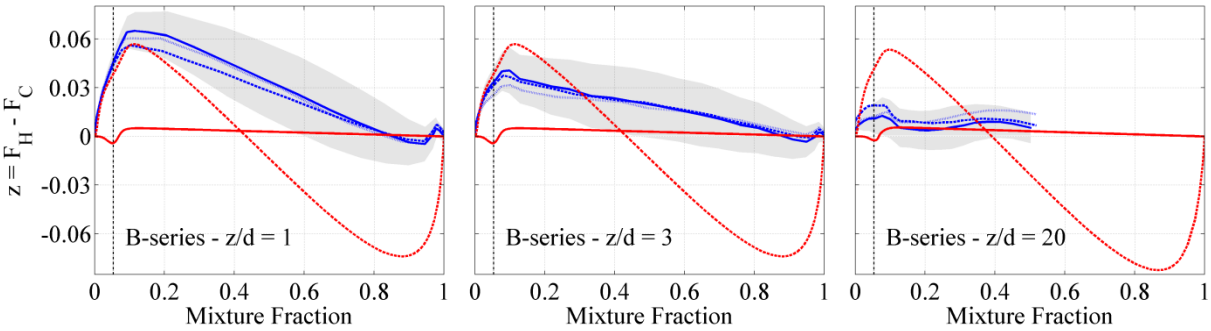

Figure 8. Differential diffusion parameter *z* plotted versus the Bilger mixture fraction for B-series flames at *z/d* = 1, 3 and 20. B-1 is shown with blue solid lines, B-2 with blue dashed lines, and B-3 with blue dotted lines. Corresponding results from laminar flame calculations using B-series fuel and oxidizer compositions with strain rates of 800 s^{-1} (left and centre) and 15 s^{-1} (right) are plotted using the two different transport regimes: full multi-component transport (red dash lines) and equal diffusivities (red solid lines). The grey area represents the conditional rms fluctuations for *z* corresponding to Flame B-1.

One way to quantify the degree of differential diffusion is to calculate the differential diffusion parameter, *z*, defined as the difference between the elemental mixture fractions of H and C; see details in [21]. Fig. 7-8 show the results for A- and B-series of flames at 1, 3 and 20 diameters above the nozzle compared to the laminar flame calculations corresponding to similar fuel and oxidizer compositions. Rms fluctuations for A-1 and B-1 are also shown.

Fig. 7-8 show that the maximum of differential diffusion parameter close to stoichiometric mixture fraction considerably decreased with the axial location, which agrees well with the theory. A second observation, especially seen at *z/d* = 1, is that the differential diffusion parameter agrees well with the full transport regime on the lean side of the reaction zone and then shows a major departure from this regime towards the equal diffusivity regime. Indeed, close to the nozzle, the reaction zone was still distant from the shear layer and located in the laminar oxidizer flow. Thus, the mixing was mostly controlled by molecular diffusion in the lean side of the flame. However, in the rich side of the reaction zone, the turbulent stirring induced by the jet flow was likely to be responsible of the behaviour of H_2 and CH_4 mass fraction in Fig. 6 and the major departure from the full molecular regime toward the equal diffusivity regime in Fig. 7-8.

Nevertheless, the differential diffusion parameter was determined by subtracting two uncertain values. Consequently, no conclusions can be made about the jet Reynolds number dependence of the differential diffusion effects in the B-series flames. In Fig. 8, the difference between the B-series measurements was not even significant compared to the rms fluctuations corresponding to Flame B-1.

Despite the high level of uncertainty of *z*, Fig. 7 seems to show a dependence of the differential diffusion with the CH_4/H_2 volume fraction. This is confirmed with the laminar flame calculations using A-1, A-2 and A-3 fuel and oxidizer compositions showing that the maximum of the differential diffusion parameter seems to decrease with lowering hydrogen in the CH_4/H_2 volume fraction. This underlines the relative importance of differential diffusion effects in flames where H_2 is mixed with a heavier gas in the fuel stream.

CO measurements

CO Raman conditional mean of mass fraction could locally reach up to 0.18 (see Fig. 3, Flame B-1 at z/d = 3), there is no N_2 present, and fluorescence can be corrected reasonably well. Consequently, CO-Raman measurements are of good quality and are reported here in favour of the CO-LIF measurements. Additionally, measurements of pure cold CO were added to the calibration procedure to optimize the accuracy of the calibration. In methane flames, the CO-LIF measurements are used in favour of the CO-Raman measurements, and the CO calibration is done in a fuel-rich, premixed laminar flame in order to minimize uncertainty in the effects of collisional quenching.

The high CO mass fractions result from high CO_2-dilution levels. Previous investigations [24, 25] have concluded that CO_2 was not inert but competed primarily with O_2 for atomic hydrogen and lead to formation of CO through the reaction $CO_2 + H \leftrightarrow CO + OH$. CO would then be expected to reach higher concentrations in the near-field compared to air-dilution. Another conclusion was that the rate of the reaction converting CO_2 into CO would decrease as the turbulent mixing rates increase up to reaching the forward rate of this reaction. The conditional mean of CO mass fraction showed in Fig. 3 for the B-series seemed to agree with this trend, especially in the near-field.

Measurement limits

During the measurements, flames displayed trends concerning soot formation at the flame tip (see Fig. 2). By reducing the H_2 content in fuel, A-series flames produced visible soot farther upstream, in part due to lower speeds at the jet exit (see Table 1), the correspondingly longer residence time for soot formation, and the higher carbon species concentration. A similar trend was revealed with B-series flames while lowering Re_{Fuel}. As seen in Fig. 2, soot formation actually reached dramatic levels in Flame A-3.

The magnitude and spectroscopic distributions of hydrocarbon fluorescence interference on the Raman measurements vary in these flames, depending on fuel composition, Reynolds number, and spatial location. Generally, measured interference levels increased with downstream distance in each flame, due to increasing residence time. At a given downstream location, fluorescence interference decreased with increasing H_2 fuel fraction and with increasing Reynolds number.

Corrections for these hydrocarbon fluorescence interferences are not perfect and leave some residual errors, particularly in regions of high interference on the fuel-rich side of the reaction zone. This can be seen, for example, in O_2 and CO mass fraction results (see Fig. 3), which can be over- or under corrected by around 1%, often appearing as a wrinkle in the plots. Similarly, an unrealistic wrinkle tended to appear for O_2 mass fraction in Fig. 3-4 and 6 and for *z* in Fig. 7-8, corresponding to mixture fractions close to 1. This is most likely due to the Raman cross-talk of CH_4 onto O_2, which is sensitive to very slight fluctuations where CH_4

is present in large quantities. This consequently affected other species mass fraction.

Results on the whole displayed reasonable accuracy, from 1 up to 20 nozzle diameters above the nozzle. Though levels of hydrocarbon fluorescence were fairly high in some cases, the sensitivity of the detection system also allowed capturing precise hydrogen mass fractions which would make this data relatively interesting for validation of turbulent combustion models. Only a limited part of the results is shown in the present paper and but most data, including scalar fluctuations and conditional statistics are available upon request.

Conclusions

Measurements of the temperature and mass fractions of main species were performed in turbulent non-premixed CO_2-diluted oxy-fuel jet flames, using the simultaneous line imaging of Raman/Rayleigh laser diagnostics setup at Sandia National Laboratories. Two series of three flames burning mixtures of hydrogen and methane in a coflow burner were studied. The objective was to investigate the influence of H_2 content in fuel and jet Reynolds number on localized extinction and flame structure in CO_2-diluted oxy-fuel flames.

Consequences of localized extinction in the flame composition could be captured, notably by the scatter plots of temperature versus mixture fraction at different axial locations. Additionally, higher contents of oxygen on the rich side of the flame front could be observed in the conditional mean of O_2 mass fraction as one progress towards higher probability of localized extinction. Based on the pdf's of the temperature, an index able to quantify the degree of extinction in the present flames was calculated as a fully burning probability.

Comparison of conditional mean mass fractions and laminar flame calculations using similar fuel and oxidizer compositions underlined the significant level of differential diffusion in the near-field that is due to the absence of turbulence in the reaction zone so close to the nozzle. The relative importance of differential diffusion tended to decrease farther downstream as the large-scale turbulent structures tended to develop and control the local mixing rates by stirring the reaction zone.

Due to the high CO_2 content in the oxidizer, CO mass fraction was found to be effectively higher than in comparable air-fuel flames, especially in the near-field. This effect would be due to CO_2 competing primarily with O_2 for atomic hydrogen and leading to formation of CO through the reaction $CO_2 + H \leftrightarrow CO + OH$. This effect seemed to be diminished out farther downstream.

Further investigations are to be done with the experimental results, notably for the CO-LIF and OH PLIF results. Besides, more detailed investigation on differential diffusion could be of importance in both flame series since Re_{Fuel} remained close to transition of molecular transport regimes. An investigation at much higher Re_{Fuel} would have been even more beneficial but remained physically unfeasible at laboratory scale due to the consequent supply of O_2 and CO_2.

Acknowledgements

The current research project has been supported by SINTEF Energy research, the Norwegian University of Science and Technology, and Sandia National Laboratories. This publication forms a part of the BIGCO2 project, coordinated by SINTEF and performed under the strategic Norwegian research program Climit. The authors acknowledge the partners: Statoil, GE Global Research, Statkraft, Aker Kværner, Shell, TOTAL, ConocoPhillips, ALSTOM, the Research Council of Norway (178004/I30 and 176059/I30) and Gassnova (182070) for their support. Sandia National Laboratories is a multi-program laboratory operated by Sandia Corporation, a Lockheed Martin Company, for the United States Department of Energy under contract DE-AC04-94-AL85000. The authors also gratefully acknowledge R. Harmon for his contributions in these experiments.

References

[1] O. Bolland; S. Saether, *Energy Conversion and Management* 33 (5-8) (1992) 467-475.

[2] O. Bolland; P. Mathieu, *Energy Conversion and Management* 39 (16-18) (1998) 1653-1663.

[3] Y. Tan; M. A. Douglas; K. V. Thambimuthu, *Fuel* 81 (8) (2002) 1007-1016 Pii S0016-2361(02)00014-5.

[4] M. Ditaranto; J. C. Sautet; J. M. Samaniego, *Experiments in Fluids* 30 (3) (2001) 253-261.

[5] J. C. Sautet; M. Ditaranto; J. M. Samaniego; O. Charon, *International Communications in Heat and Mass Transfer* 26 (5) (1999) 647-656.

[6] J. C. Sautet; L. Salentey; M. Ditaranto, *International Communications in Heat and Mass Transfer* 28 (2) (2001) 277-287.

[7] E. Croiset; K. V. Thambimuthu, *Fuel* 80 (14) (2001) 2117-2121.

[8] T. Boushaki; J. C. Sautet, *Experiments in Fluids* 48 (6) (2010) 1095-1108 DOI 10.1007/s00348-009-0788-1.

[9] M. Ditaranto; J. Hals, *Combustion and Flame* 146 (3) (2006) 493-512 DOI 10.1016/j.combustflame.2006.04.015.

[10] F. H. V. Coppens; A. A. Konnov, *Fuel* 87 (13-14) (2008) 2866-2870 DOI 10.1016/j.fuel.2008.04.009.

[11] P. Kutne; B. K. Kapadia; W. Meier; M. Aigner, *Proceedings of the Combustion Institute* 33 (2) (2011) 3383-3390.

[12] R. S. Barlow; J. H. Frank; A. N. Karpetis; J. Y. Chen, *Combustion and Flame* 143 (4) (2005) 433-449 DOI 10.1016/j.combustflame.2005.08.017.

[13] R. S. Barlow; H. C. Ozarovsky; A. N. Karpetis; R. P. Lindstedt, *Combustion and Flame* 156 (11) (2009) 2117-2128 DOI 10.1016/j.combustflame.2009.04.005.

[14] D. C. Haworth, *Progress in Energy and Combustion Science* 36 (2) (2010) 168-259 DOI 10.1016/j.pecs.2009.09.003.

[15] R. S. Barlow; G. H. Wang; P. Anselmo; M. S. Sweeney; S. Hochgreb, *Proceedings of the Combustion Institute* 32 (2009) 945-953 DOI 10.1016/j.proci.2008.06.070.

[16] F. Fuest; R. S. Barlow; D. Geyer; F. Seffrin; A. Dreizler, *Proceedings of the Combustion Institute* 33 (1) (2011) 815-822.

[17] D. Geyer, *1D-Raman/Rayleigh Experiments in a Turbulent Opposed-Jet*, PhD Thesis, TU Darmstadt, VDI-Verlag, Düsseldorf (2005) ISBN 3-18-353306-5.

[18] R. W. Bilger; S. H. Starner; R. J. Kee, *Combustion and Flame* 80 (2) (1990) 135-149.

[19] CHEMKIN-PRO, Reaction Design: San Diego, 2008.

[20] G. P. Smith; D. M. Golden; M. Frenklach; N. W. Moriarty; B. Eiteneer; M. Goldenberg; C. T. Bowman; R. K. Hanson; S. Song; W. C. Gardiner; V. V. Lissianski; Z. Qin, http://www.me.berkeley.edu/gri_mech/.

[21] R. S. Barlow; G. J. Fiechtner; C. D. Carter; J. Y. Chen, *Combustion and Flame* 120 (4) (2000) 549-569.

[22] W. Meier; A. O. Vyrodov; V. Bergmann; W. Stricker, *Applied Physics B-Lasers and Optics* 63 (1) (1996) 79-90.

[23] V. Bergmann; W. Meier; D. Wolff; W. Stricker, *Applied Physics B-Lasers and Optics* 66 (4) (1998) 489-502.

[24] A. R. Masri; R. W. Dibble; R. S. Barlow, *Combustion and Flame* 91 (3-4) (1992) 285-309.

[25] P. Glarborg; L. L. B. Bentzen, *Energy & Fuels* 22 (1) (2008) 291-296 Doi 10.1021/Ef7005854.